Stacking faults and the γ-surface on $\{1\bar{1}01\}$ pyramidal planes in α-titanium

A. J. Ready and A. P. Sutton*
Department of Physics, Imperial College London, Exhibition Road, London, SW7 2AZ, United Kingdom

P. D. Haynes
Department of Materials, Imperial College London, Exhibition Road, London, SW7 2AZ, United Kingdom

D. Rugg
Rolls-Royce plc, Elston Rd., Derby DE24 8BJ, United Kingdom

Using first principles methods we calculated the entire γ-surface of the first order pyramidal planes in α-titanium. Slip on these planes involving dislocations with $\mathbf{c}+\mathbf{a}$ dislocations is one means by which α-titanium polycrystals may supplement slip on prism planes with $\mathbf{a}$-type Burgers vectors to maintain ductility. We find two stable intrinsic stacking faults with relatively small energies. We show that dissociation of $\mathbf{c}+\mathbf{a}$ dislocations into two dislocations with Burgers vectors $(\mathbf{c}+\mathbf{a})/2$ is not possible in α-titanium because there is no stable stacking fault at $(\mathbf{c}+\mathbf{a})/2$. Instead we propose a possible dissociation of a $\mathbf{c}+\mathbf{a}$ dislocation into three partial dislocations separated by the two intrinsic faults we have identified.

PACS numbers: 61.72.Nn, 62.20.fk, 62.20.fq, 61.50.Ah

I. Introduction

Titanium and its alloys are used in the aerospace industry owing to their high specific strength, fatigue resistance and corrosion resistance[1]. α-titanium has a hexagonal close packed (hcp) crystal structure and it may deform plastically either by slip or twinning. The primary slip planes are $\{1\bar{1}00\}$ prism planes shown in red in Fig. 1 with Burgers vectors $\langle\mathbf{a}\rangle = (1/3)\langle\bar{1}\bar{1}20\rangle$ in the basal plane[1]. There are only two such independent prism slip systems. At least three additional independent slip systems are required to accommodate an arbitrary deformation, according to the von Mises criterion. More general deformation may be accommodated by twinning, when it is not suppressed by alloying. Alternatively, it may be accommodated by '$\langle\mathbf{c}+\mathbf{a}\rangle$ slip' with Burgers vector $\mathbf{c}+\mathbf{a} = \frac{1}{3}[1\bar{2}13]$ on the $(01\bar{1}1)$ first-order pyramidal plane shown in green in Fig. 1 or on $\{11\bar{2}2\}$ second-order pyramidal planes. There are four independent $\langle\mathbf{c}+\mathbf{a}\rangle$ slip systems on first-order pyramidal planes; with the two independent prism slip systems the von Mises criterion is satisfied.

$\langle\mathbf{c}+\mathbf{a}\rangle$ dislocations are frequently observed in experiments where single α-Ti crystals are deformed in tension along the $\mathbf{c}$-axis, and in polycrystals[2–5]. These dislocations have been observed predominantly on $\{01\bar{1}1\}$ planes but they have also been observed on $\{11\bar{2}2\}$ planes. Paton et al.[2] and Minonishi et al.[3] found that $\mathbf{c}$-axis deformation in α-Ti single crystals below 300°C was predominantly accommodated by twinning with $\langle\mathbf{c}+\mathbf{a}\rangle$ slip ahead of the propagating twins. Above 400°C deformation was accommodated by a combination of twinning and $\langle\mathbf{c}+\mathbf{a}\rangle$ slip. Numakura et al.[5] found that all deformation in α-Ti polycrystals along the $\mathbf{c}$-axis was accommodated by $\langle\mathbf{c}+\mathbf{a}\rangle$ slip. They also suggested that $\langle\mathbf{c}+\mathbf{a}\rangle$ dislocations may dissociate because the Burgers vector is so large. Tomsett and Bevis observed a dissociation of $\langle\mathbf{c}+\mathbf{a}\rangle$ dislocations into a pair of $(1/2)\langle\mathbf{c}+\mathbf{a}\rangle$ partial dislocations in Zn[6,7]. We are unaware of any experimental evidence for such a dissociation in α-Ti.

$\langle\mathbf{c}+\mathbf{a}\rangle$ dislocations have recently been observed in molecular dynamics (MD) simulations of a Mg single crystal strained along the $\mathbf{c}$-axis. Tang and El-Awady[8]

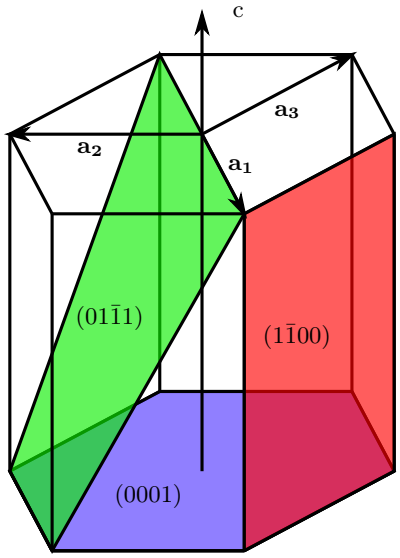

Figure 1: (Colour online) Some slip planes in α-Ti. The critical resolved shear stress at room temperature is smallest on the prism plane (red) with Burgers vector $\langle\mathbf{a}\rangle$, followed by the basal plane (blue) with Burgers vector $\langle\mathbf{a}\rangle$, and the first-order pyramidal plane (green) for slip with Burgers vector $\langle\mathbf{c}+\mathbf{a}\rangle$[1].

observed that $\langle \mathbf{c}+\mathbf{a} \rangle$ dislocations nucleate via the formation of two partial dislocations: a leading partial with Burgers vector $(1/9)[\bar{3}\bar{2}5\bar{6}]$ and a trailing partial $(1/9)[0\bar{1}1\bar{3}]$.

When a perfect dislocation dissociates into partial dislocations there are stacking faults between them. The fault vectors correspond to local minima of an energy surface called the γ-surface[9]. For a given lattice plane normal $\hat{\mathbf{n}}$ one half of the crystal is translated rigidly with respect to the other half by $\mathbf{t}$, where $\mathbf{t} \cdot \hat{\mathbf{n}} = \mathbf{0}$. The γ-surface is the energy $\gamma(\mathbf{t})$ of the generalised stacking fault with fault vector $\mathbf{t}$. For a rational plane translational symmetry limits the inequivalent set of fault vectors $\mathbf{t}$ to those within the Wigner-Seitz cell of the two-dimensional lattice in the plane. Point group symmetry may reduce the set of inequivalent fault vectors further. Allowing atomic relaxation only along $\hat{\mathbf{n}}$ the energy $\gamma(\mathbf{t})$ of the fault is calculated at absolute zero. This procedure works particularly well when the spacing of lattice planes with normal $\hat{\mathbf{n}}$ is relatively large. As the lattice plane spacing decreases atomic relaxations parallel to the fault may become increasingly important, in addition to those normal to the fault. It is then essential to carry out a fully unconstrained relaxation of any fault that corresponds to a local minimum of $\gamma(\mathbf{t})$ to see whether the minimum still exists and whether its translation vector $\mathbf{t}$ changes. A further complication arises in crystals where each lattice site is associated with more than one atom, such as hcp, because there may be more than one distinct separation between atomic planes sharing the same normal. In these circumstances the location of the fault plane is not unique.

The first-order pyramidal plane $\{01\bar{1}1\}$ is the plane on which $\langle \mathbf{c}+\mathbf{a} \rangle$ slip is most often seen in α-Ti[5,7,10]. There are two spacings of atomic $\{01\bar{1}1\}$ planes in an hcp crystal. In this paper we use first principles methods to compute the entire γ-surface for a generalised fault lying between $\{01\bar{1}1\}$ atomic planes with the larger spacing.

Domain and Legris[11] and Kwasniak et al.[12] calculated line sections of the γ-surface for the $\{01\bar{1}1\}$ plane along $\mathbf{a}$ and $\mathbf{c}+\mathbf{a}$ using DFT and a $3p^6 3d^2 4s^2$ pseudopotential for α-Ti. Their results for generalised faults between widely spaced planes are in good agreement. The $\mathbf{c}+\mathbf{a}$ line section of the $\{10\bar{1}1\}\gamma$-surface of α-Zr calculated by Domain and Legris[11] is very similar to that of α-Ti, with a local minimum at $\approx \frac{1}{2}(\mathbf{c}+\mathbf{a})$. However, the energy of the minimum was considered[11] probably too high to lead to dissociation of a dislocation with Burgers vector $\mathbf{c}+\mathbf{a}$ into two with Burgers vectors $\approx \frac{1}{2}(\mathbf{c}+\mathbf{a})$.

Liang[13] proposed a dissociation of a $\mathbf{c}+\mathbf{a}$ dislocation based on his stacking fault energy calculations using DFT and the nudged elastic band (NEB) method. He proposed a $\langle \mathbf{c}+\mathbf{a} \rangle$ dissociation into three partials with Burgers vectors $0.19[2\bar{1}\bar{1}\bar{3}]$, $0.215[10\bar{1}\bar{2}]$ (the twinning direction on the $(10\bar{1}1)$ plane), and $0.072[1\bar{2}10]$. The $(1/3)[1\bar{2}10]$ vector can lie either in the $(10\bar{1}1)$ plane or the $(10\bar{1}0)$ plane.

The entire γ-surfaces between both narrowly and widely spaced atomic $\{01\bar{1}1\}$ planes have been calculated for α-Zr using DFT and an embedded atom potential[14]. They found the maximum energies in the γ-surface for the narrowly spaced planes were much higher than for the widely spaced planes. Ghazisaeidi et al.[15] calculated the γ-surface for the narrowly spaced atomic $\{01\bar{1}1\}$ planes in α-Ti using a modified embedded atom potential, and compared the line section of the surface along $\mathbf{a}$ with DFT. Poty et al.[16] also calculated entire γ-surfaces between closely spaced first order pyramidal planes in α-Ti and α-Zr using classical interatomic potentials, as well as along the $\langle \mathbf{c}+\mathbf{a} \rangle$-type direction using DFT. Their results agree qualitatively with the results of Ghazisaeidi et al., but differ quantitatively.

In this paper we present DFT and interatomic potential calculations of entire γ-surfaces in α-Ti on the basal plane and between widely spaced first order pyramidal planes. The entire γ-surface on the basal plane in α-Ti has already been computed using DFT[17] and this provides a useful comparison. As far as we know the entire γ-surface between widely-spaced first order pyramidal planes in α-Ti has not been previously published. The computational methods are set out in section II, the γ-surfaces are presented in section III, the discussion of these results follows in section IV, and we conclude in section V. Additional details concerning the convergence tests carried out in support of the results of this study are detailed in appendices A and B.

II. Methods

A. DFT/MD parameters

All DFT results in this paper were obtained using CASTEP version 8.0[18]. We used two types of ultrasoft pseudopotential for Ti[19]. The first was the pseudopotential with 12 valence electrons in the $3s^2 3p^6 3d^2 4s^2$ ground state configuration (denoted 12elPP) generated by the CASTEP on-the-fly pseudopotential generation tool. The second was the 4 valence electron pseudopotential (4elPP) in the $3d^2 4s^2$ ground state configuration generated by White[20]. The PBE exchange-correlation functional[21] was used for all calculations.

A plane wave energy cut-off of 480 eV for the 12elPP and 650 eV for the 4elPP enabled the error in the total energy arising from the incomplete basis set to be reduced to 3 meV/atom. Convergence to 0.5 meV/atom was reached with a 23x23x15 $\mathbf{k}$-point mesh for the primitive unit cell using both pseudopotentials. We used the cold smearing scheme[22] to improve computational efficiency with a smearing width of 0.1 eV. We computed energy volume curves for α-Ti and fitted them to the Birch-Murnaghan equation of state[23,24] to determine $a = 2.94$ and $c/a = 1.580$. DFT relaxations were deemed complete when the maximum force on any atom was less than 10 meV/Å, and the total electronic energy was converged to within 0.01 meV per atom.

All MD calculations were carried out using

LAMMPS[25] and the interatomic potential (IP) generated by Ackland[26]. The IP was used with the equilibrium lattice parameters for which the potential was constructed, i.e. $a = 2.97$ and $c/a = 1.592$. IP relaxations were deemed complete when the maximum force on an atom was less than 0.01 meV/Å.

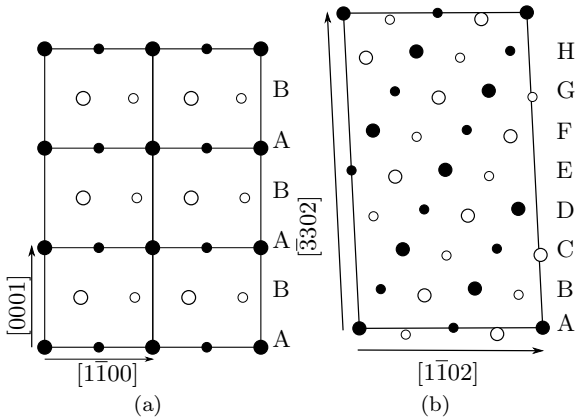

Figure 2: (Colour online) Projected views along [11$\bar{2}$0] direction of the hcp crystal to illustrate the stacking sequences (a) ... ABAB ... of (0002) basal planes and (b) ... ABCDEFGH ... of (1$\bar{1}$0$\bar{1}$) pyramidal planes. Small and large circles distinguish atoms on adjacent (11$\bar{2}$0) planes. Black and white atoms distinguish atoms on the two hexagonal sublattices in the hcp structure.

B. Supercell geometries: basal

Three dimensional periodic boundary conditions were applied to a supercell comprising 14 atomic basal planes. The smallest rectangular repeat cell in the (0001) plane is bounded by (1/3)[11$\bar{2}$0] and [1$\bar{1}$00] lattice vectors (see Fig. 2(a)). This cell contains two lattice sites, one associated with the four corners and one in the centre. A primitive periodic cell in the plane of the generalised fault was selected for the γ-surface calculation, bounded by (1/3)[11$\bar{2}$0] and (1/3)[2$\bar{1}\bar{1}$0]. The γ-surface was sampled using a 78 point uniform grid in this primitive cell. Each supercell contained two equivalent generalised stacking faults with equal and opposite translation vectors. The faults were separated by 7 (0002) planes. See Appendix A for details of convergence tests.

C. Supercell geometries: first-order pyramidal

For the γ-surface on the (1$\bar{1}$0$\bar{1}$) first order pyramidal plane a slab geometry was used with the generalised faults in the middle of each slab. Three-dimensional periodic boundary conditions were applied with 26.8 Å vacuum between the slabs. The smallest rectangular repeat cell in the (1$\bar{1}$0$\bar{1}$) plane is bounded by (1/3)[11$\bar{2}$0] and [1$\bar{1}$02] lattice vectors. This cell also contains two lattice sites. Exploiting the mirror symmetry normal to [11$\bar{2}$0] and translational symmetry of the lattice only a quarter of the rectangular cell has to be sampled to construct the full γ-surface; the cell bounded by $\frac{1}{6}$[11$\bar{2}$0] and $\frac{1}{2}$[1$\bar{1}$02] was sampled by a uniform 4×12 uniform grid for both the DFT and IP calculations. However, for the 12elPP γ-surface a uniform grid of only 24 points was used. The normal to (1$\bar{1}$0$\bar{1}$) is not a lattice vector, but a nearby lattice vector is [3$\bar{3}$0$\bar{2}$]. In each [3$\bar{3}$0$\bar{2}$] repeat there are eight (1$\bar{1}$0$\bar{1}$) lattice planes and sixteen (1$\bar{1}$0$\bar{1}$) atomic planes (see Fig. 2(b)). The spacings of (1$\bar{1}$0$\bar{1}$) atomic planes alternate between small and large. Following Ackland[26] a pair of closely spaced atomic planes is called a 'superplane'. The slab contained one generalised stacking fault between a pair of adjacent superplanes. Each period of the slab comprised 48 atoms arranged in 12 superplanes.

Before the faults were introduced the slab was relaxed fully. When the generalised stacking faults were introduced the two superplanes furthest from and on either side of the fault were allowed to displace only rigidly normal to the fault, i.e. to float.

See Appendix B for details of the pyramidal convergence tests carried out in support of this study.

Results	ISFE (mJ/m^2)
DFT (this work)	306
DFT[17]	259
DFT[11,15]	292
TB[27,28]	290-370
BO[29]	110
IP (this work)	65
ZM[17]	54
ZM[30]	56
HKV[17]	65
A-FS[29]	64
MEAM[31]	170-172
Experiment[32]	>300

Table I: Intrinsic stacking fault energies (ISFE) on the basal plane computed in this work and elsewhere compared with experiment. Results have been separated into DFT, tight binding (TB), bond order potential (BO), interatomic potentials (IP, ZM, HKV, A-FS, MEAM).

III. Results

A. The basal γ-surface

The γ-surfaces computed for the basal plane using DFT with the 12elPP and an IP[26] are shown in Fig. 3. The local minimum at $\frac{1}{3}$[10$\bar{1}$0] on each γ-surface, and its translational equivalent at $\frac{1}{3}$[10$\bar{1}$0] + $\frac{1}{3}$[11$\bar{2}$0] = $\frac{1}{3}$[21$\bar{3}$0], corresponds to the intrinsic stacking fault. The corresponding intrinsic stacking fault energies (ISFEs) are compared with published calculated and experimental values[11,16,17] in Table I. It is striking that the interatomic potentials underestimate the ISFE by up to a factor of five compared with experiment and DFT calculations.

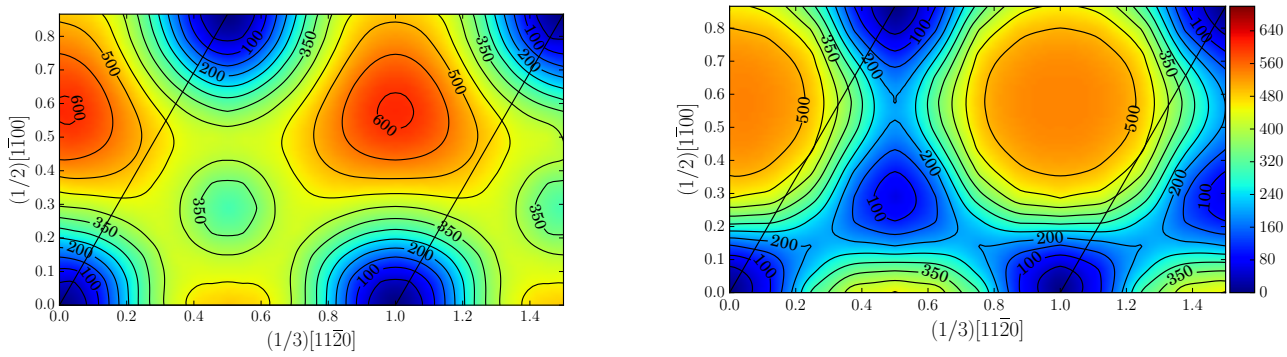

Figure 3: (Colour online) The γ-surface for the basal plane computed using (a) DFT with the 12elPP and (b) an IP[26]. While the positions of the local maxima and minima are the same in the two γ-surfaces they have smaller energies in the IP γ-surface. All energies are expressed in mJ/m^2. The contours are spaced by 50 mJ/m^2. A primitive unit cell in the basal plane is outlined in black.

B. The first-order pyramidal γ-surface

The γ-surface computed using DFT and the 4elPP is shown in Fig. 4(a). The surface is broadly similar to the α-Zr γ-surface computed by Chaari et al.[14]. However, the local minimum at [0.5, 0.27] in Fig. 4(a) is absent in Chaari et al.'s γ-surface.

The γ-surface computed using DFT and the 12elPP is very similar to that computed with the 4elPP. Figure 4(c) shows the difference $\gamma_{12elPP}(\mathbf{t}) - \gamma_{4elPP}(\mathbf{t})$ between the 12elPP and 4elPP γ-surfaces. This gives a measure of the error associated with using the 4elPP instead of the 12elPP. The dark blue colouring of the entire surface indicates that the error is small throughout. Indeed, the root mean square difference is 30 mJ/m^2. However near to the local maxima at $[0, 0.4]$ and $[0.5, 0.12]$, the energy difference reaches -60 mJ/m^2 and 40 mJ/m^2. The positions of the local minima in the γ-surface remained unchanged with the 12elPP.

The vector at the centre of the γ-surfaces shown in Fig. 4 is $\frac{1}{3}[2\bar{1}\bar{1}3]$, which is a $\mathbf{c} + \mathbf{a}$ lattice vector. The energy of the γ-surface at that point is therefore zero. In Fig. 4(a) there are only two distinct local minima, located at $[0.00, 0.21]$ and $[0.50, 0.27]$. These are quite close to what Ackland[26] called 'intrinsic' and 'extrinsic' stacking fault configurations respectively. However, the term 'extrinsic' is not appropriate here since the fault may be created by relative translation at a single plane, and it does not require insertion or removal of material. Since they are both intrinsic faults we label them I_1 and I_2 respectively.

Figure 5 shows the fully relaxed slab obtained with the 12elPP. The structure consists of a contiguous array of octahedra and tetrahedra, examples of which are shown by 'o' and 't'. The free $(1\bar{1}0\bar{1})$ surfaces at the top and bottom of the slab undergo small inward relaxations, and their structures also comprise contiguous arrays of slightly distorted octahedra and tetrahedra. When the generalised stacking faults are introduced between the 6th and 7th superplanes the bottom two superplanes and top two superplanes are allowed to float rigidly, but the atoms within those 4 superplanes are not allowed to undergo any further independent relaxation.

Fig. 6 shows the atomic structure of the fully relaxed I_1 fault obtained with the 12elPP. The atomic structure of the fault comprises a contiguous array of octahedra shown by 'o'. The superplanes adjacent to the fault are less rumpled than in the bulk.

Fig. 7 shows the atomic structure of the fully relaxed I_2 fault obtained with the 12elPP. Part of the displacement associated with this fault is along the direction of projection, which transforms small circles into large circles and vice versa. As a result the atomic structure of the fault comprises an array of trigonal prisms and tetrahedra, shown by 'p' and 't'.

The energies of the I_1 and I_2 faults are given in Table II. The energies of the fully relaxed I_1 and I_2 faults are almost the same when computed with either the 4elPP or the 12elPP. There are large differences in the energies of both faults obtained by DFT between (i) relaxation displacements constrained to be normal to the fault plane only and (ii) unconstrained relaxation displacements (see Table II). These differences are around a factor of two. To investigate the source of these large differences we compared the structures of the faults obtained by DFT using the 12elPP with constrained and full relaxations.

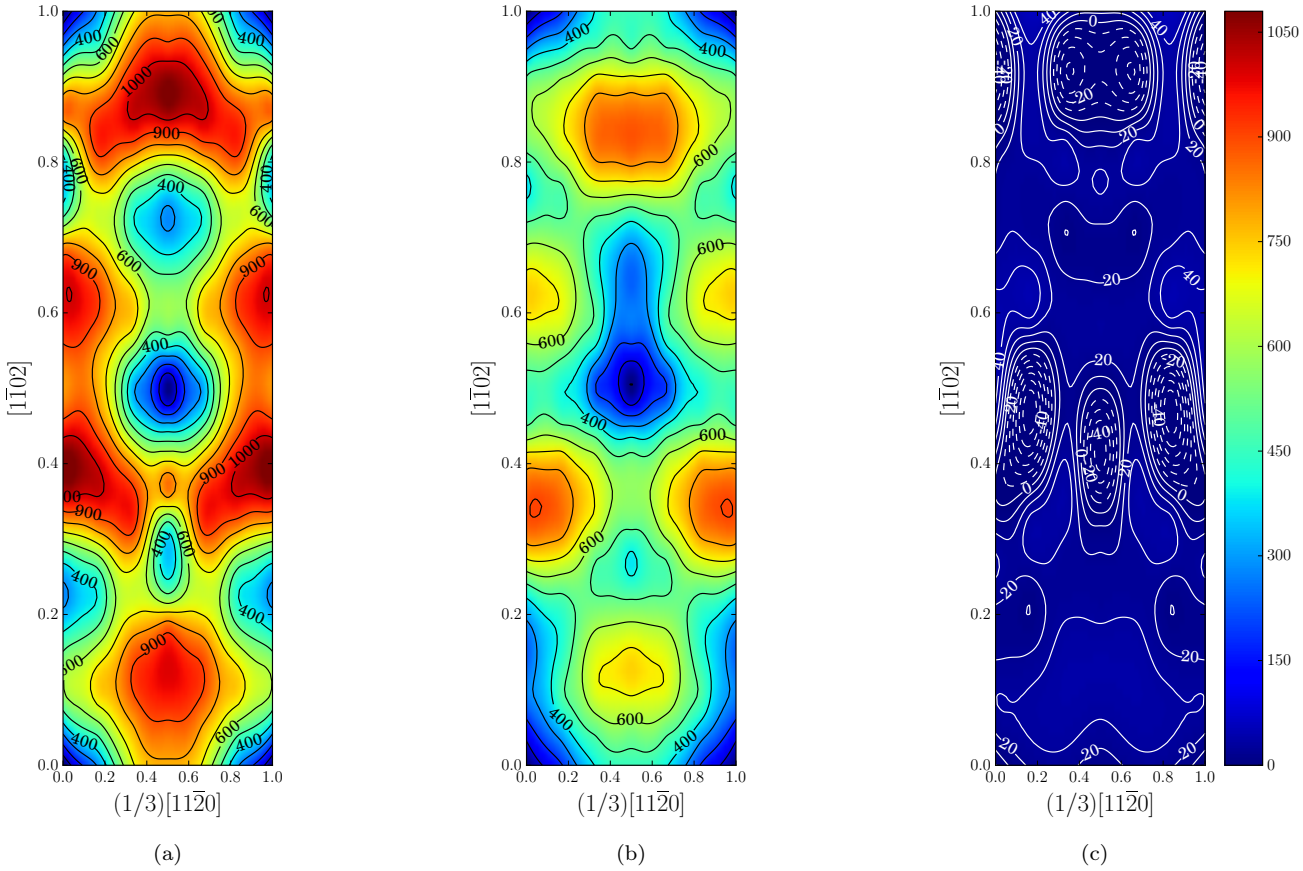

Figure 4: (Colour online) γ-surfaces of the first-order pyramidal plane computed using (a) DFT with the 4elPP and (b) an IP[26]. The energy scale for both γ-surfaces is shown on the right. All energies are expressed in mJ/m^2, and the contours are separated by 100 mJ/m^2. The difference between the DFT γ-surfaces computed with the 4elPP and 12elPP is plotted in (c), where the contours are separated by 10 mJ/m^2, and contours of negative energy are shown by broken lines.

The differences were extremely small, with changes in the translation vector parallel to the I_1 fault of $[0.00, 0.02]$ Å, and a contraction perpendicular to the fault of 0.10 Å. There were no changes in the translation vector parallel to the I_2 fault, and a contraction perpendicular to the fault of 0.01 Å. Changes in the individual atomic displacements in both faults were less than 0.14 Å when the relaxation constraints were removed.

There is a local minimum in the γ-surface obtained with the IP shown in Fig. 4(b) at $[0.0, 0.15]$, which we associate with the I_1 fault, but it is revealed only by the local darker shade of blue colouring, not by the contours. However, when a finer sampling grid of 32×96 is used, instead of the 4×12 grid, and halving the contour spacing to 50 mJ/m^2, the resulting γ-surface reveals the local minimum clearly with an energy of 233 mJ/m^2. The energy reduced to 225 mJ/m^2 when an unconstrained relaxation was performed.

There is also a local minimum in the γ-surface obtained with the IP at [0.5,0.26], which we associate with the I_2 fault. It has an energy of 377 mJ/m^2, which reduced to 351 mJ/m^2 when an unconstrained relaxation was carried out.

The changes in the energies of the faults between the constrained and unconstrained relaxations were much less for the IP than for the DFT calculations. The relaxation displacements of the constrained and fully relaxed systems differed by as much as 0.11 Å in the I_1 case and 0.17 Å in the I_2 case. These relaxations occurred parallel to the fault. Displacements perpendicular to the fault differed by less than 0.02 Å for both faults.

IV. Discussion

The very large difference between the intrinsic SF energies on the basal plane calculated with DFT and the IP is most likely due either to the fitting procedure for the IP or a more fundamental limitation arising from its inability to capture the directional nature of d-bonding in α-Ti, as discussed by Girshick et al.[33] Using the 12elPP we find the energy of the stacking fault on the basal plane is 306 mJ/m^2.

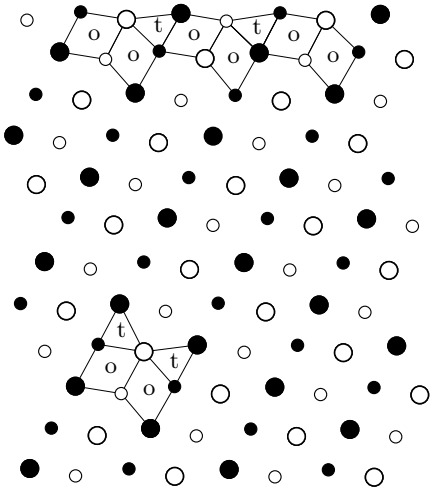

Figure 5: Two periods of the fully relaxed unfaulted slab obtained with the 12elPP, viewed in projection along $[11\bar{2}0]$. Examples of octahedra and tetrahedra are shown by 'o' and 't'. The colouring and the sizes of the circles follow the same scheme as in Fig. 2.

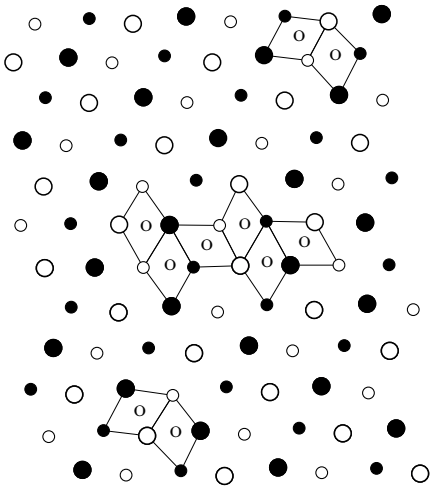

Figure 6: Two periods of the fully relaxed I_1 stacking fault on the $(1\bar{1}0\bar{1})$ plane, obtained with the 12elPP, viewed in projection along $[11\bar{2}0]$. 'o' and 't' label octahedra and tetrahedra that make up the fault.

For the γ-surface of the first-order pyramidal plane, as calculated with DFT using both pseudopotentials, there are two local minima, I_1 and I_2 at $[0.00, 0.21]$ and $[0.50, 0.27]$ respectively. Using the 12elPP we find their energies are 163 and 160 mJ/m^2. Although the translation states of these faults parallel and perpendicular to the fault changed by no more than 0.14 Å when an unconstrained relaxation is carried out, small local changes in the atomic structures lead to substantial reductions in their energies. These local minima occur at slightly different locations with the IP: $I_1 = [0.00, 0.15]$ and $I_2 = [0.50, 0.26]$ with energies 233 and 377 mJ/m^2 respectively, which reduce to 225 and 351 mJ/m^2 with an unconstrained relaxation.

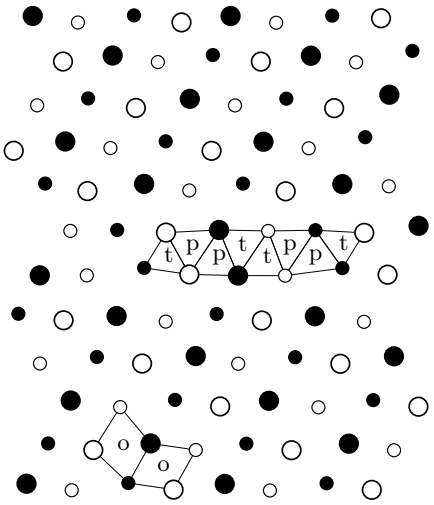

Figure 7: Two periods of the fully relaxed I_2 stacking fault on the $(1\bar{1}0\bar{1})$ plane, obtained with the 12elPP, viewed in projection along $[11\bar{2}0]$. 'p' and 't' label trigonal prisms and tetrahedra that make up the fault.

Results	I_1		I_2	
	Full	Con	Full	Con
12elPP (this work)	163	288	160	282
4elPP (this work)	150	279	148	341
10elPP[13]	134	243	-	-
IP (this work)	225	233	351	377
IP[26]	314	-	435	-

Table II: The energies of the I_1 and I_2 intrinsic faults for the first-order pyramidal plane computed with DFT and three pseudopotentials, and with an IP generated by Ackland[26]. 'Full' indicates an unconstrained ionic relaxation allowing atomic displacements parallel and normal to the fault plane. 'Con' indicates a constrained ionic relaxation allowing displacements only normal to the fault plane. All energies in mJ/m^2.

To investigate the differences between the 4elPP and the 12elPP γ-surfaces for the first order pyramidal plane (see Fig. 4(c)) we searched for the smallest nuclear separations in the atomic configurations corresponding to the largest energy differences between the 4elPP and 12elPP results. The largest energy differences occur at $p_1 = (1/6, 1/2)$ and $p_2 = (1/2, 9/22)$ on the γ-surfaces. We found the smallest separation with the 4elPP for p_1 was 2.74 Å and for p_2 it was 2.75 Å, and they occurred at the fault and at the free surface. These are 0.14 Å and 0.13 Å smaller than the smallest nuclear separation in the perfect crystal. Twice the core radius for the 4 electron pseudopotential is 2.54 Å. Since the wavelength of electrons at 480 eV is 0.56 Å the 'core radius' has a finite width of about 0.28 Å. Therefore, when atoms come closer than $2.54 + 0.28 = 2.82$ Å the distinction between valence and core electrons begins to break down. Since

2.75 Å is less than 2.82 Å this is the likeliest reason for the discrepancies between the 4elPP and 12elPP γ-surfaces.

The existence of two local minima in the γ-surface of the first order pyramidal plane has implications for a possible dissociation of a $\mathbf{c}+\mathbf{a}$ dislocation. In Fig. 9 the Burgers vector of the lattice dislocation $\mathbf{b} = \mathbf{c}+\mathbf{a} = \frac{1}{2}(\frac{1}{3}[11\bar{2}0] + [1\bar{1}02]) = \frac{1}{3}[2\bar{1}\bar{1}3]$ is shown by the white arrow. It is possible that this dislocation could dissociate into three partial dislocations with Burgers vectors $\mathbf{b}_1, \mathbf{b}_2, \mathbf{b}_3$, shown by the black arrows in Fig. 9, with I_1 fault between $\mathbf{b}_1$ and $\mathbf{b}_2$ and I_2 fault between $\mathbf{b}_2$ and $\mathbf{b}_3$:

$$\begin{aligned}
\mathbf{b} = \mathbf{c}+\mathbf{a} &= \frac{1}{3}[2\bar{1}\bar{1}3] \\
&= \mathbf{b}_1 + \mathbf{b}_2 + \mathbf{b}_3 \\
\mathbf{b_1} &\approx \frac{4}{18}[1\bar{1}02] \\
\mathbf{b_2} &\approx \frac{1}{6}[11\bar{2}0] + \frac{1}{18}[1\bar{1}02] = \frac{1}{18}[42\bar{6}2] \\
\mathbf{b_3} &\approx \frac{4}{18}[1\bar{1}02]. \qquad (1)
\end{aligned}$$

A similar dissociation was found in simulations by Tang and El-Awady[8] of the nucleation of $\mathbf{c}+\mathbf{a}$ dislocations in Mg using embedded atom potentials. Whether this dissociation occurs in Ti depends on the anisotropic elastic energies and core energies of the dissociated and undissociated dislocations as well as the intrinsic fault energies.

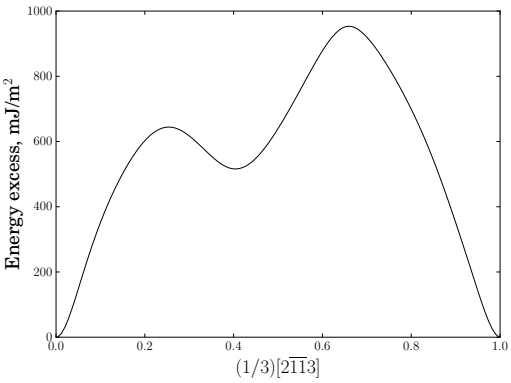

Figure 8: A line section of the 4elPP pyramidal γ-surface shown in Fig. 4(a) along the straight line between [0,0] and [0.5,0.5]. The point [0.5,0.5] on the γ-surface corresponds to a translation of $\frac{1}{3}[2\bar{1}\bar{1}3]$.

It should be noted that the dissociation of a $\mathbf{c}+\mathbf{a}$ dislocation into two with Burgers vectors $(\mathbf{c}+\mathbf{a})/2$ is not possible because there is no stable stacking fault at $[0.25, 0.25]$ in the γ-surface. The translation corresponding to the $\mathbf{c}+\mathbf{a} = \frac{1}{3}[2\bar{1}\bar{1}3]$ Burgers vector is represented by the centre of the γ-surface (i.e. [0.5,0.5]) in Fig. 4. If a line section is taken from a corner to the centre of the γ-surface a local minimum is found at $\approx [0.2, 0.2]$, as shown in Fig. 8. However, this is not a true minimum, as may be seen in the full γ-surface in Fig. 4(a).

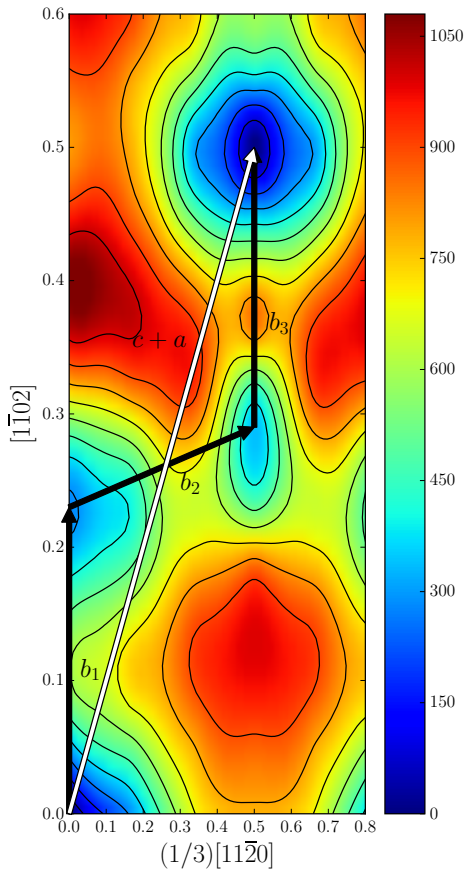

Figure 9: (Colour online) A section of the first-order pyramidal γ-surface shown in Fig. 4(a) with a decomposition of the $\langle \mathbf{c}+\mathbf{a} \rangle$ Burgers vector (shown in white) into three partial Burgers vectors (shown in black.) All energies are expressed in mJ/m^2.

V. Conclusions

Using DFT we have computed the full γ-surfaces of the basal and first order pyramidal planes in α-titanium. Our results for the basal plane are in good agreement with earlier published γ-surfaces obtained by DFT, and we obtained an energy of approximately 300 mJ/m^2 for the intrinsic stacking fault energy. For the first order pyramidal plane we found two intrinsic stacking faults, with energies of approximately 160 mJ/m^2. We identified a possible dissociation of a $\mathbf{c}+\mathbf{a}$ dislocation into three partial dislocations separated by these two intrinsic faults. We do not find a metastable fault near $(\mathbf{c}+\mathbf{a})/2$.

The 4elPP provides a fair description of titanium provided atomic separations are not less than 2.82 Å.

The interatomic potential by Ackland[26] reproduces the main features obtained by DFT of the γ-surfaces of both the basal and first order pyramidal planes, but the energies of metastable faults differ very significantly from those obtained by DFT.

Acknowledgements

AJR was supported through a studentship in the Centre for Doctoral Training on Theory and Simulation of Materials at Imperial College funded by EPSRC under Grant No. EP/G036888/1. Additional support was provided by Rolls-Royce plc. We thank the Thomas Young Centre and the Imperial College High Performance Computing Centre.

Appendix A: Convergence tests for γ-surfaces on the basal plane

Using periodic boundary conditions, as described in section II B, the intrinsic stacking fault energy (ISFE) on the basal plane was calculated in periodic cells containing $\{6, 10, 14, 18, 22, 26\}$ atomic layers using DFT and the IP. The results are shown in Table III, where it is seen that the cell containing 14 layers yields an ISFE within 2 % of those computed using larger cells. This cell size was therefore deemed sufficient. The ISFE is well converged with just 6 layers in the periodic cell when atomic interactions are described by the IP. Interactions between the faults are longer-ranged with DFT.

Table III: The ISFE in mJ/m^2 on the basal plane as a function of the number of atomic layers in the periodic cell.

Number of layers	DFT ISFE	IP ISFE
6	326.9	64.6
10	314.9	-
14	306.0	64.5
18	303.4	-
22	301.2	64.5
26	302.7	-

Appendix B: Convergence tests for γ-surfaces on the first order pyramidal plane

Table IV: The relaxation energies in eV of the pyramidal surfaces and an unstable SF for the 4 and 12-electron pseudopotentials in slabs with different numbers of superplanes.

Number of Superplanes	12elPP	4elPP
4	1.59	1.56
6	1.57	1.50
8	1.67	1.38
10	1.65	1.32
12	1.48	1.28
14	1.47	1.29
16	1.45	1.26

To determine the minimum acceptable thickness of the slab for the calculation of the γ-surface using DFT we selected the generalised fault corresponding to the global maximum at $[0.0, 0.4]$ of the γ-surface. By varying the thickness of slabs containing this fault we identified the thickness required for the energies of the fault and the two surfaces to be converged. Since this a convergence test for the γ-surface, relaxation displacements were confined to the fault normal. Slab thicknesses ranging from 4 to 16 superplanes (16 to 64 atoms) were considered.

Table IV lists the reductions in the total energy of slabs that started as slabs of perfect crystal with no relaxation. For both pseudopotentials a slab of 12 superplanes has a relaxation energy within 2% of the relaxation energies of the two larger slabs.

Fig. 10 shows the interplanar spacings in the [0.0,0.4] generalised fault following the constrained relaxations. There is a large expansion at the fault, and contractions at the two surface layers, with oscillations in the superplane spacing in between. These oscillations decay and almost vanish in the slab with 16 superplanes. The configurations obtained with both pseudopotentials are reasonably well converged with 12 superplanes, particularly with the 12elPP.

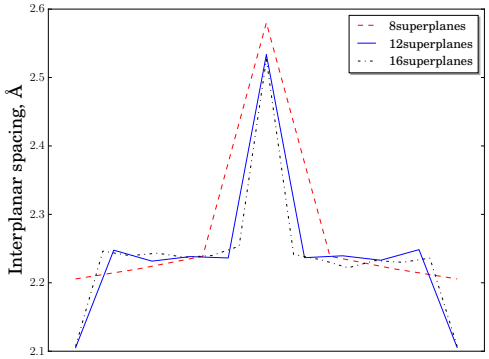

(a)

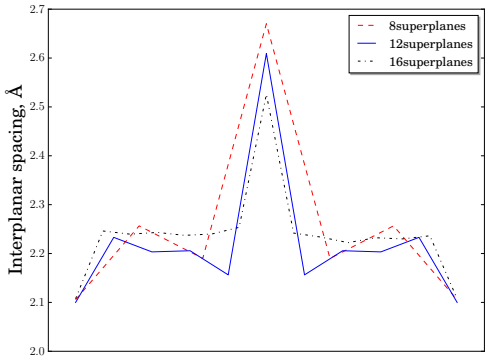

(b)

Figure 10: The interplanar spacings through slabs of 8, 12 and 16 superplanes after constrained relaxations. (a) shows the 12elPP results, and (b) shows the 4elPP results.

* a.sutton@ic.ac.uk

[1] G. Lutjering and J. C. Williams, *Titanium*, Vol. 2 (Springer, 2003).
[2] N. E. Paton and W. A. Backofen, Metallurgical Transactions **1**, 2839 (1970).
[3] Y. Minonishi, S. Morozumi, and H. Yoshinaga, Scripta Metallurgica **16**, 427 (1982).
[4] I. P. Jones and W. B. Hutchinson, Acta Metallurgica **29**, 951 (1981).
[5] H. Numakura, Y. Minonishi, and M. Koiwa, Scripta Metallurgica **20**, 1581 (1986).
[6] D. I. Tomsett and M. Bevis, Philosophical Magazine **19**, 129 (1969).
[7] M. H. Yoo, J. R. Morris, K. M. Ho, and S. R. Agnew, Metallurgical and Materials Transactions A **33**, 813 (2002).
[8] Y. Tang and J. A. El-Awady, Acta Materialia **71**, 319 (2014).
[9] V. Vítek, Philosophical Magazine **18**, 773 (1968).
[10] Q. Yu, J. Sun, J. W. Morris, and A. M. Minor, Scripta Materialia **69**, 57 (2013).
[11] C. Domain and A. Legris, IUTAM Symposium on Mesoscopic Dynamics of Fracture Process and Materials Strength , 411 (2004).
[12] P. Kwaśniak, P. Śpiewak, H. Garbacz, and K. J. Kurzydłowski, Physical Review B - Condensed Matter and Materials Physics **89**, 144105 (2014).
[13] L. Liang, *Simulation ab initio des defauts etendus du Ti α en presence d'interstitiels H et O*, Ph.D. thesis, Ecole Polytechnique, Universite Paris-Saclay, Route de Saclay, 91128 Palaiseau, France (2016), liang Liang's PhD Thesis.
[14] N. Chaari, E. Clouet, and D. Rodney, Metallurgical and Materials Transactions A: Physical Metallurgy and Materials Science **45**, 5898 (2014), arXiv:1410.1121.
[15] M. Ghazisaeidi and D. R. Trinkle, Acta Materialia **60**, 1287 (2012).
[16] A. Poty, J. M. Raulot, H. Xu, J. Bai, C. Schuman, J. S. Lecomte, M. J. Philippe, and C. Esling, Journal of Applied Physics **110** (2011), 10.1063/1.3599870.
[17] M. Benoit, N. Tarrat, and J. Morillo, Modelling and Simulation in Materials Science and Engineering **21**, 015009 (2013), arXiv:1206.2490.
[18] S. J. Clark, M. D. Segall, C. J. Pickard, P. J. Hasnip, M. I. J. Probert, K. Refson, and M. C. Payne, Z. Kristallogr. **220**, 567 (2005).
[19] D. Vanderbilt, Physical Review B **41**, 7892 (1990).
[20] J. White, "Ti_00.uspcc," `http://cmt.dur.ac.uk/Pseudopotentials/Ti_00.uspcc` (1998), [Online; accessed 22-June-2016].
[21] J. P. Perdew, K. Burke, and M. Ernzerhof, Phys. Rev. Lett. **77**, 3865 (1996).
[22] M. Methfessel and A. T. Paxton, Physical Review B **40**, 3616 (1989).
[23] F. D. Murnaghan, Proceedings of the National Academy of Sciences **30**, 244 (1944).
[24] F. Birch, Physical Review **71**, 809 (1947).
[25] S. Plimpton, "Fast Parallel Algorithms for Short-Range Molecular Dynamics," (1995).
[26] G. J. Ackland, Philosophical Magazine A **66**, 917 (1992).
[27] P. B. Legrand, Philosophical Magazine A **52**, 83 (1985).
[28] P. B. Legrand, Philosophical Magazine B **49**, 171 (1984).
[29] A. Girshick, A. M. Bratkovsky, D. G. Pettifor, and V. Vitek, Philosophical Magazine A **77**, 981 (1998).
[30] R. Zope and Y. Mishin, Physical Review B **68**, 024102 (2003).
[31] R. G. Hennig, T. J. Lenosky, D. R. Trinkle, S. P. Rudin, and J. W. Wilkins, Physical Review B - Condensed Matter and Materials Physics **78**, 1 (2008), arXiv:0706.1764.
[32] P. Partridge, Metallurgical Reviews **12**, 169 (1967).
[33] A. Girshick, D. G. Pettifor, and V. Vitek, Philosophical Magazine A **77**, 37 (1998).